Effect of carbonation-drying-wetting on durability of coral aggregate seawater concrete

Da Bo[1,2,3,4]　　Yu Hongfa[5]　　Ma Haiyan[5]　　Dou Xuemei[5]　　Wu Zhangyu[5]　　Chen Yan[1]

([1] College of Harbour, Coastal and Offshore Engineering, Hohai University, Nanjing 210098, China)
([2] Yangtze Institute for Conservation and Development, Hohai University, Nanjing 210098, China)
([3] Nantong Institute of Marine and Offshore Engineering, Hohai University, Nantong 226300, China)
([4] Key Laboratory of Coastal Disaster and Defence of Ministry of Education, Hohai University, Nanjing 210098, China)
([5] Department of Civil Engineering, Nanjing University of Aeronautics and Astronautics, Nanjing 210016, China)

Abstract: Based on the drying-wetting cycles experiment and the carbonation-drying-wetting cycles experiment for coral aggregate seawater concrete (CASC) with different strength grades, the effects of carbonation-drying-wetting on the durability of CASC are studied with the surface state, mass loss rate, relative dynamic elastic modulus, ultrasonic wave velocity and cube compressive strength as indices. Results show that the mass loss rate of CASC increases gradually with the increase in cycle times in the drying-wetting and carbonation-drying-wetting cycles. The mass loss rate increases relatively slowly at the initial stage but it increases remarkably after 10 cycles. The relative dynamic elastic modulus and ultrasonic wave velocity decrease gradually with the increase in cycle times. After 6 cycles, the decrease rate of the relative dynamic elastic modulus and ultrasonic wave velocity of CASC tends to be flat and the surface is slightly damaged. Compared with the initial 28 d cube compressive strength, the cube compressive strength of CASC decreases by 8.8% to 11.0%. Drying-wetting cycles and carbonation can accelerate seawater erosion on CASC, and drying-wetting cycles result in salting-out and accelerate the destruction of concrete. Therefore, the carbonation-drying-wetting accelerates the destruction of CASC.

Key words: coral aggregate seawater concrete; drying-wetting cycles; carbonation-drying-wetting cycles; mass loss rate; relative dynamic elastic modulus; ultrasound wave velocity

DOI: 10.3969/j.issn.1003 – 7985.2021.01.009

High temperature, high humidity, high salinity and windy tropical marine environment will corrode the structure of coral aggregate seawater concrete (CASC)[1-3]. However, drying-wetting cycles, carbonation and Cl⁻ erosion mainly affect the durability of marine concrete[4-7]. Drying-wetting cycles can cause the expansion and stripping of concrete. Carbonation destroys the alkaline environment of concrete, leading to steel corrosion and the failure of concrete structures[8]. Cl⁻ in seawater causes chemical erosion on concrete and also leads to steel corrosion and concrete cracks[9]. Therefore, for marine engineering construction, it is of great engineering value and theoretical significance to study the effect of carbonation-drying-wetting on the durability of CASC.

Kakooei et al.[10] studied the steel corrosion and Cl⁻ diffusion behavior of CASC, finding that the polarization resistance of CASC is significantly lower than that of ordinary aggregate concrete (OAC) at the same concrete mix proportion, and that the Cl⁻ diffusion and steel corrosion rate of CASC are significantly higher than those of OAC. Yu et al.[1,11] made a field investigation of CASC structure on Xisha island, finding that the tropical marine environment has a strong corrosive effect on C15-C25 CASC structure. Its carbonation depth and steel corrosion rate are relatively high. Da et al.[12] studied the Cl⁻ diffusion behavior of CASC, finding that the Cl⁻ diffusion of CASC is characterized by high initial Cl⁻ content, high surface Cl⁻ content and high Cl⁻ diffusion coefficient. Wang et al.[13] studied the feasibility of steel tube CASC, finding that the problem of Cl⁻ erosion can be effectively avoided by pouring CASC into the steel tube. In addition, the calculation model of the axial compressive bearing capacity of steel tube CASC column is established. Da et al.[14-15] studied the steel corrosion behavior of CASC, explored the mechanism of steel corrosion degradation in CASC, and proposed an anti-corrosion technology of steel in CASC with low cost and high durability. In conclusion, there are no in-depth studies on the durability of CASC at present. Therefore, this paper studies the effects of carbonation-drying-wetting cycles on the durability of CASC.

Based on 14 times of the drying-wetting cycles experiment and carbonation-drying-wetting cycles experiment for CASC with different strength grades, the surface state, mass loss rate (W_1), relative dynamic elastic modulus (E_r), ultrasonic wave velocity (V_t) and cube compressive strength (f_{cu}) are referred to as evaluation indices to study the effect of carbonation-drying-wetting on the durability of CASC. This serves as a reference for the research on the degradation mechanism and engineering application of CASC.

1 Experiment

1.1 Raw materials

Coral and coral sand are taken from South China Sea

(see Fig. 1), and the mechanical properties of coral aggregate are shown in Tab. 1. P · Ⅱ 52.5 Portland cement is produced by Jiangnan Onoda Cement Co., Ltd. Grade Ⅰ fly ash (FA) is produced by the Thermal Power Plant, and S95 ground slag (SG) is produced by Jiangnan Grinding Co., Ltd. The chemical compositions of the cement and mineral admixtures are shown in Tab. 2. Polycarboxylic acid high performance water-reducer is produced by Jiangsu Bote New Material Co., Ltd., in which Na_2SO_4 is 0.18% (mass percent, the same below), Cl^- is 0.01%, solid content is 30%, and the water reduction rate is 25%. Seawater is prepared in accordance with ASTM D1141-2013, containing $NaCl$: Na_2SO_4 : $MgCl_2 \cdot 6H_2O$: KCl : $CaCl_2 = 24.5 : 4.1 : 11.1 : 0.7 : 1.2$.

Tab. 1 Mechanical properties of coral aggregate

Materials	Bulk density/ ($kg \cdot m^{-3}$)	Apparent density/ ($kg \cdot m^{-3}$)	Void ratio/%	Water absorption rate/%	Cl^- content/%	Fineness modulus
Coral	1 062	2 557	58.5	10.9	0.074	
Coral sand	1 391	2 500	45.0	11.1	0.112	2.44

Tab. 2 Chemical compositions of cement and mineral admixtures   %

Materials	$w(SiO_2)$	$w(Al_2O_3)$	$w(CaO)$	$w(MgO)$	$w(SO_3)$	$w(Fe_2O_3)$
Cement	21.35	4.67	62.60	3.08	2.25	3.31
FA	54.88	26.89	4.77	1.31	1.16	6.49
SG	28.15	16.02	34.54	6.03	0.32	1.13

1.2 Specimen preparation

The size of CASC is 100 mm × 100 mm × 100 mm, and its mix proportion is shown in Tab. 3. First, cement,

coral, coral sand, SG, FA and water-reducer are dried in a mixer for 1 min, and then mixed with seawater for 3 min. The slump of concrete is measured after discharging, and then poured and shaped by vibration. After the completion of CASC, wet cloth is used to cover the surface of CASC. After 24 h, the mould is removed and the CASC is placed in the room of (20 ± 2)℃. The drying-wetting cycles experiment and carbonation-drying-wetting cycles experiment of CASC are tested after 28 d maintenance with a straw cover and sprayed with seawater.

Tab. 3 Mix proportion of CASC

No.	$m(cement)$/ kg	$m(SG)$/ kg	$m(FA)$/ kg	$m(coral sand)$/ kg	$m(coral)$/ kg	$m(water)$/ kg	$m(water-reducer)$/ kg	R_1	R_2	Slump/mm
C50	275	150	75	873	582	296	8.3	0.30	0.59	125
C60	620	120	60	860	369	221	6.0	0.20	0.28	120
C65	780	150	70	700	300	250	6.0	0.25	0.20	255

Note: R_1 represents the mass of net water to that of cement, slag and fly ash; R_2 represents the mass of total water to that of cement, slag and fly ash; total water includes the net water and pre-absorption water.

1.3 Experimental method

According to EN1992-1-1 (2004), W_1 is 5%, E_r is decreased to 60%, and the loss of f_{cu} is 25%, which are referred to as the failure standards. Based on the drying-wetting cycles experiment and carbonation-drying-wetting cycles experiment for CASC with different strength grades, the durability of CASC is studied according to the surface state, W_1, E_r, V_t and f_{cu}.

1.3.1 Seawater immersion experiment

CASC is immersed in seawater relatively for 30, 78 and 120 d, and the seawater solution is changed every 28 d.

1.3.2 Drying-wetting cycles experiment

According to GB/T 50082—2009, the drying-wetting cycle system is as follows (see Tab. 4).

Step 1 Place the CASC in seawater solution which is at least 20 mm above its surface. The time from the beginning to the immersion end is 2 d. The seawater solution is changed every 28 d, and the temperature of the seawater solution is controlled at 25-30 ℃.

Step 2 After immersion, the CASC is taken out, for air-drying in a ventilated place, and then drying in an oven. The heating is completed within 30 min, and the temperature is maintained at 50 ℃. The time from heating to cooling is 2 d.

Step 3 After drying, the CASC is cooled immediately

and aired in the ventilated place for 2 d.

Step 4 The test lasts 84 d in total with a 6 d cycle operating 14 times. At the end of every 2 drying-wetting cycles, E_r, W_1, V_t and f_{cu} are measured.

1.3.3 Carbonation-drying-wetting cycles experiment

According to GB/T 50082—2009, the carbonation-drying-wetting cycle system is as follows (see Tab. 4).

Tab. 4 The cycle system of the experiment

No.	Experiment	Cycle system
P	Seawater immersion	Seawater immersion for 30, 78 and 120 d
PG	Drying-wetting cycle	Seawater immersion for 2 d, drying for 2 d and air-drying for 2 d
PT	Carbonation-drying-wetting cycle	Seawater immersion for 2 d, drying for 2 d and carbonation for 2 d

Steps 1-2 are the same as those of the drying-wetting cycles experiment.

Step 3 After drying, the CASC is cooled to room temperature. The CASC is instantly carbonized in the CCB-70A carbonation chamber. Carbonation time is 2 d, temperature is (20 ± 3) ℃, relative humidity is $(70 \pm 10)\%$ and CO_2 concentration is $(20 \pm 3)\%$.

Step 4 The test lasts 84 d in total with a 6 d cycle operating for 14 times. At the end of every 2 carbonation-drying-wetting cycles, E_r, W_1, V_t and f_{cu} are measured.

Step 5 To test the carbonation depth, the CASC is placed on a test pressure machine, and the residual powder is scraped off after splitting. Phenolphthalein solution with a concentration of 1% is dripped on it. After 30 s, the carbonation depth is measured with a depth caliper every 10 mm along the section. The average value of the carbonation depth at each measuring point is taken as the carbonation depth of CASC.

1.3.4 Analysis method

E_r of CASC is measured by NM-4B non-metallic ultrasonic testing analyzer. The calculation model[16] is as follows:

$$E_r = \frac{V_t^2}{V_0^2} \times 100\% \tag{1}$$

where E_r is the relative dynamic elastic modulus, %; V_0 is the initial ultrasonic wave velocity, km/s; V_t is the ultrasonic wave velocity after t d of erosion, km/s.

f_{cu} of CASC is measured according to the rebound value with the concrete rebound hammer. The calculation model[17] is as follows:

$$f_{cu} = 24.612e^{0.017R} \tag{2}$$

where f_{cu} is the cube compressive strength, MPa; R is the rebound value.

W_1 of CASC is measured by an electronic balance. The calculation model is as follows:

$$W_1 = \frac{M_t - M_0}{M_0} \times 100\% \tag{3}$$

where W_1 is the mass loss rate, %; M_0 is the initial mass of concrete, kg; M_t is the mass of concrete after t d of erosion, kg.

2 Results and Discussion

2.1 Drying-wetting cycles

2.1.1 Surface state

Fig. 1 gives the surface state of CASC in the drying-wetting cycles. It shows that after 14 cycles, the high strength CASC does not show much damage on the surface. Erosion stripping can be seen on the surface of low strength CASC. This is mainly because many voids are produced by the remaining bubbles during the formation of concrete, and these voids are where erosion occurs, through which the seawater solution invades into the concrete. With the increase in cycle times, irregular small cracks appear on the edges and around the samples. The surface of the samples has white crystals, and the number of crystals of C50 is greater than that of C60 on the surface. This is mainly due to the rapid evaporation of water in the pore on the CASC surface during the drying-wetting cycles. The rapid crystallization of residual salt gives rise to pressure, resulting in cracks on the surface, which provides a channel for the solution to re-infiltrate into concrete[18]. During the wetting process of CASC, there is a large solution concentration difference between the surface and interior, which greatly accelerates the ion permeation rate under capillary absorption. Therefore, in the drying-wetting cycles, the erosion products of concrete are brought about continuously, and the long-term cumulative effect leads to white crystals on the surface, which eventually leads to the failure of concrete.
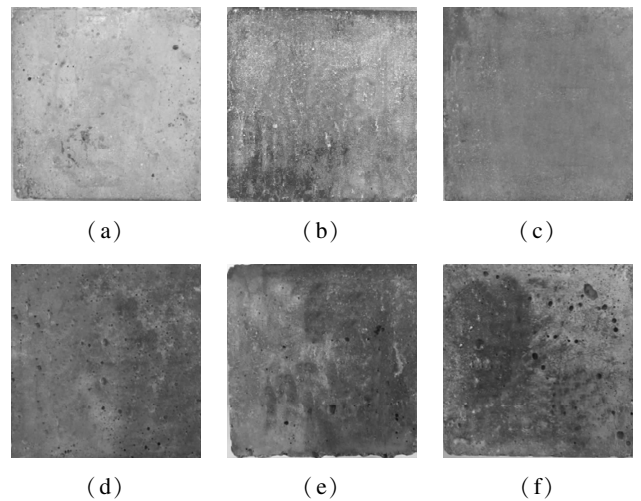

Fig. 1 Surface state of CASC in the drying-wetting cycles. (a) C50(P); (b) C60(P); (c) C65(P); (d) C50(PG-10); (e) C60 (PG-14); (f) C65(PG-14)

2.1.2 Mass loss rate

Fig. 2 gives the mass loss rate (W_1) of CASC in the drying-wetting cycles. It shows that in the 2nd, 4th, 6th and 8th drying-wetting cycles, W_1 of C65 is 0.89%,

0.90%, 1.48%, 1.63%, respectively, indicating that with the increase in cycle times, W_1 of C65 increases gradually and the rate relatively slows down. In the 10th, 12th and 14th drying-wetting cycles, W_1 of C65 is 2.22%, 3.56% and 4.59%, respectively, indicating that the growth rate of W_1 at the later stage is obviously higher than that at the initial stage. The reasons are as follows: 1) During the drying-wetting cycles, the degree of hydration of CASC is increased and its internal density is gradually enhanced. 2) Various ions diffuse into the internal pores of concrete, producing plenty of products of erosion, which compact the concrete, but there are not many products and they increase slowly. With the increase in cycle times, various corrosive ions enter the pores of concrete through capillary adsorption and natural diffusion[19], accelerating the corrosion of concrete and significantly increasing W_1 at the later stage.
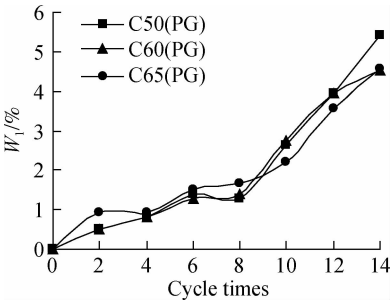

Fig. 2 W_1 of CASC in the drying-wetting cycles

2.1.3 Relative dynamic elastic modulus and ultrasonic wave velocity

Fig. 3 gives the relative dynamic elastic modulus (E_r) and ultrasonic wave velocity (V_t) of CASC in the drying-wetting cycles. It shows that E_r of CASC decreases gradually with the increase in cycle times. Furthermore, for the same cycle times, the higher the strength of CASC, the greater the E_r. In the drying-wetting cycles, with the increase in cycle times, V_t of CASC decreases gradually. V_t of C65 is the maximal, C60 is the in-between, and C50 is the minimal in the same cycle times, which is consistent with the rule of E_r.

In addition, in the 4th, 8th and 12th cycles, E_r of C65 increases by 2.80%, 2.34% and 3.68%, respectively, compared with that of C60. E_r of C60 increases by 3.55%, 2.17% and 3.95%, respectively compared with that of C50. After 14 cycles, E_r of C50, C60 and C65 decreases by 29%, 26% and 26%, respectively, which does not reach the failure threshold. The reasons are as follows: In the drying-wetting cycles, the diffusion of various ions silt up in the pores of CASC, and thus the expansion stress increases, cohesion weakens, and concrete swelling and shrinkage lead to the gradual extension of cracks from inside to outside. Damage accumulates continuously and the decrease trend of E_r gradually slows down.
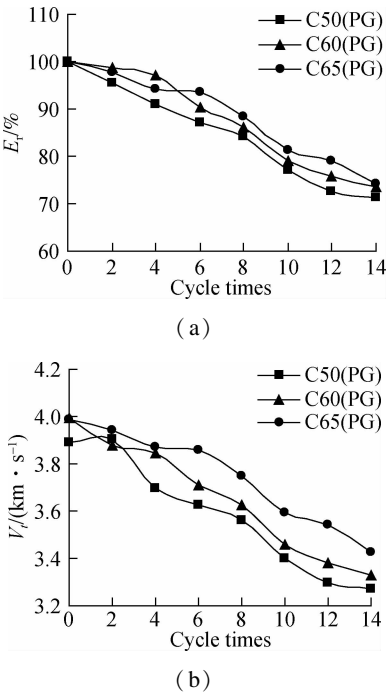

(a)

(b)

Fig. 3 E_r and V_t of CASC in the drying-wetting cycles. (a) E_r; (b) V_t

The pore structure of low strength CASC has a low compactness and high permeability, which is conducive to the growth and enrichment of erosion products, aggravating the formation of micro-cracks, and accelerating the decline rate of E_r[20].

2.1.4 Cube compressive strength

Tab. 5 gives the cube compressive strength (f_{cu}) of CASC in the drying-wetting cycles and carbonation-drying-wetting cycles, in which the curing age is 28 d. It shows that f_{cu} of C50, C60 and C65 decreases by 11.0%, 11.0% and 9.2%, respectively, after 14 cycles, which is consistent with the rule of E_r and V_t.

Tab. 5 f_{cu} of CASC in the different cycle systems

No.	f_{cu}	No.	f_{cu}
C50(PG)	57.5	C50(PT)	57.5
C60(PG)	65.4	C60(PT)	64.9
C65(PG)	69.3	C65(PT)	69.3

In addition, it shows that f_{cu} of C50, C60 and C65 decreases by 9.4%, 11.0% and 8.8%, respectively, after 14 carbonation and drying-wetting cycles, which is consistent with the rules of E_r and V_t. Besides, f_{cu} of CASC in the drying-wetting cycles and carbonation and drying-wetting cycles are compared, which essentially reflects the effect of carbonation. It shows that carbonation has no obvious effect on f_{cu} of C60 and C65, while f_{cu} of C50 slightly increases under carbonation.

2.2 Carbonation-drying-wetting cycles
2.2.1 Surface state

Fig. 4 gives the surface state of CASC in the carbona-

tion-drying-wetting cycles. It shows that after 14 cycles, the surface state of CASC does not change obviously, and there is no clear damage on the surface, but erosion stripping can be seen on the surfaces of CASC. With the increase in cycle times, irregular small cracks appear on the edges and around the samples. The surface of the samples has white crystals, and the crystal amount of C50 is greater than that of C60 on the surface. In addition, the carbonation depth of CASC is measured by the phenolphthalein reagent, as shown in Fig. 4(d). The test results are shown in Tab. 6. It can be seen that only C50 is carbonized but C60 and C65 are not. After 14 cycles, the carbonation depth of C50 CASC reaches 6.12 mm.
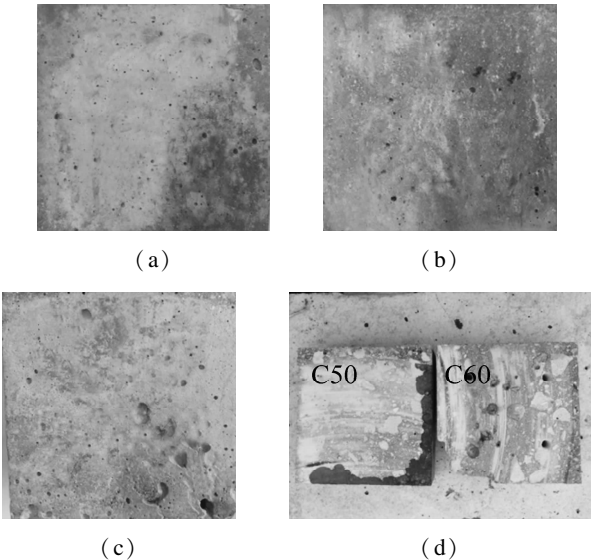

(a)   (b)

(c)   (d)

Fig. 4 Surface state of CASC in the carbonation-drying-wetting cycles. (a) C50(PT-10); (b) C60(PT-10); (c) C65(PT-10); (d)Carbonation depth

Tab. 6 Carbonation depth of CASC   mm

Cycle times	2	4	6	8	10	12	14
C50(PT)	0.75	2.51	2.82	3.03	3.13	5.56	6.12
C60(PT)	0	0	0	0	0	0	0
C65(PT)	0	0	0	0	0	0	0

2.2.2 Mass loss rate

Fig. 5 gives W_1 of CASC in the carbonation-drying-wetting cycles. It shows that with the increase in cycle times, W_1 of CASC increases gradually, and the growth rate of W_1 at the initial stage is relatively slow. During the 4th-10th cycle times, the growth rate of W_1 increases. After 12 cycles, the growth rate of W_1 tends to be flat. For the same cycle times, W_1 of low strength CASC is significantly higher than that of high strength CASC. Besides, in the 8th, 10th, 12th and 14th cycles, W_1 of C50 is 1.88%, 2.20%, 2.79% and 3.01%, respectively; W_1 of C60 is 1.36%, 1.51%, 2.57% and 2.87%, respectively; and W_1 of C60 decreases by 0.52%, 0.69%, 0.22% and 0.14%, respectively, compared with that of C50. This indicates that in the carbonation-drying-wetting cycles, the ions invading inside CASC can fill the pores,

and their compactness increases gradually with the hydration and carbonation of cement. The lower the strength of CASC, the greater the permeability, and the higher the growth rate of W_1. With the increase in cycle times, W_1 tends to be flat or even slightly decreases, indicating that erosion products fasten the formation of micro-cracks and aggravate the damage, but the decrease of W_1 is not obvious because the damage is slight. If the cycle times is prolonged, the interior of CASC will be damaged more seriously or even destroyed, and W_1 will decrease significantly.
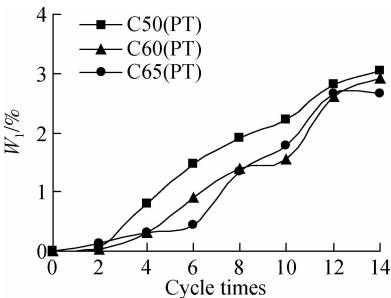

Fig. 5 W_1 of CASC in the carbonation-drying-wetting cycles

Fig. 6 gives W_1 of CASC in the carbonation-drying-wetting cycles. It shows that W_1 of CASC in the carbonation-drying-wetting cycles is lower than that in the drying-wetting cycles. After 10 cycles, the difference of W_1 between the two cycle modes increases gradually, indicating slowdown in the weight gain of CASC at the carbonation later stage. The reasons are that in the carbonation-drying-wetting cycles, W_1 not only gives rise to salt erosion and physical crystallization, but also exacerbates the damage in concrete, including permeability and cracks, especially in low strength concrete[21-22].
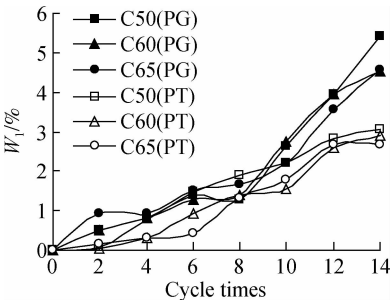

Fig. 6 W_1 of CASC in the different cycle systems

2.2.3 Relative dynamic elastic modulus and ultrasonic wave velocity

Fig. 7 gives E_r and V_t of CASC in the carbonation-drying-wetting cycles. It shows that E_r of CASC decreases gradually with the increase in cycle times, and tends to be flat after 6 cycles. For the same cycle times, E_r of CASC increases gradually with the increase in CASC strength. In addition, V_t of CASC decreases with the increase in cycle times. For the same cycle times, V_t of C65 is the

maximal, C60 is the in-between, and C50 is the minimal, which is consistent with the rule of E_r. In the 4th, 8th, 10th and 14th cycles, E_r of C65 is 5.92%, 7.20%, 4.06% and 5.40%, respectively, which are higher than that of C60. E_r of C60 is 7.28%, 4.34%, 4.30% and 2.64%, respectively, which are higher than that of C50. After 14 cycles, E_r of C50, C60 and C65 decreases by 34.72%, 32.08% and 26.68%, respectively, which does not reach the failure threshold.
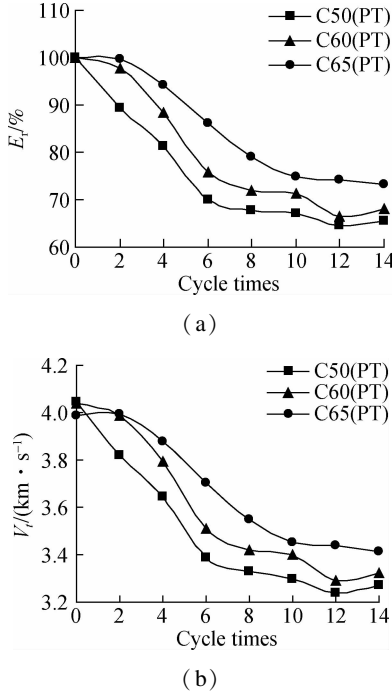

Fig. 7 E_r and V_t of CASC in the carbonation-drying-wetting cycles. (a) E_r; (b) V_t

According to the mechanism of Cl$^-$ erosion[23-24], Cl$^-$ diffuses into CASC through capillary pores and cracks, and the diffusion or permeation rate is influenced by porosity, pore structure, environmental temperature, etc. In addition, the carbonation-drying-wetting cycles also provide conditions for Cl$^-$ erosion: 1) In the drying-wetting cycles, the temperature rises, the concentration of ions entering CASC increases rapidly, and the chemical reaction accelerates, which increases the number of erosion products and accelerates the damage of CASC. 2) Carbonation also changes the pore structure of CASC and makes it easy for the solution to invade CASC[25]. Therefore, the carbonation-drying-wetting cycles accelerate the destruction of CASC.

Fig. 8 gives E_r and V_t of CASC in the carbonation-drying-wetting cycles. It shows that carbonation-drying-wetting cycles accelerate the decrease of E_r and V_t of CASC, and aggravate damage inside CASC. In addition, C50 and C60 change clearly, but C65 does not. The reasons are that the higher the strength of CASC, the more reasonable the distribution of its micro-structure. Also, to

some extent, the salt erosion is not always bad, because the products of erosion can fill the pores of CASC, which increases the solid volume of the structure, improves the internal pore structure and enhances the strength of CASC.
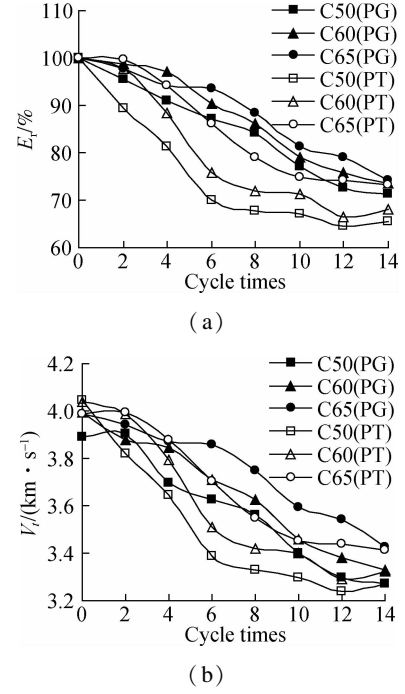

Fig. 8 E_r and V_t of CASC in the different cycle systems. (a) E_r; (b) V_t

By comparing the effects of the two cycle modes on E_r and V_t, it is shown that the rate of durability deterioration of CASC in the carbonation-drying-wetting cycles is significantly higher than that in the drying-wetting cycles, and the lower the strength of CASC, the faster the decline of E_r and V_t.

3   Conclusions

1) In the drying-wetting cycles and carbonation-drying-wetting cycles, with the increase in cycle times, W_1 of CASC increases gradually, and the growth rate of W_1 at the initial stage is relatively slow. After 10 cycles, W_1 of CASC increases remarkably faster. In addition, W_1 of C65 is smaller than that of C50 after 10 cycles.

2) In the drying-wetting cycles and carbonation-drying-wetting cycles, with the increase in cycle times, E_r and V_t of CASC decrease gradually, and tend to be flat after 6 cycles. For the same cycle times, V_t of C65 is the maximal, C60 is the in-between, and C50 is the minimal. In the carbonation and drying-wetting cycles, the decrease in E_r of C50 is significantly higher than that in the drying-wetting cycles, while E_r of C65 decreases by almost the same extent in the two cycle modes.

3) In the drying-wetting cycles and carbonation-drying-wetting cycles, f_{cu} of CASC decreases. Compared with

the initial 28 d f_{cu}, f_{cu} of CASC decreases by 8.8% to 11.0%. In the carbonation and drying-wetting cycles, only C50 is carbonized but C60 and C65 are not. After 14 cycles, the carbonation depth of C50 CASC reaches 6.12 mm.

4) Drying-wetting cycles and carbonation can accelerate seawater erosion on CASC, and drying-wetting cycles result in the salting-out and accelerate destruction of concrete. Therefore, carbonation-drying-wetting accelerates the destruction of CASC.

References

[1] Yu H F, Da B, Ma H Y, et al. Durability of concrete structures in tropical atoll environment[J]. *Ocean Engineering*, 2017, **135**: 1−10. DOI:10. 1016/j. oceaneng. 2017. 02. 020.

[2] Da B, Yu H F, Ma H Y, et al. Reliability of service life of coral aggregate seawater concrete structure in tropic island reef environment[J]. *Journal of the Chinese Ceramic Society*, 2018, **46**(11): 1613−1621. DOI:10. 14062/j. issn. 0454-5648. 2018. 11. 16. (in Chinese)

[3] Da B, Yu H F, Ma H Y, et al. Experimental investigation of whole stress-strain curves of coral concrete[J]. *Construction and Building Materials*, 2016, **122**: 81−89. DOI:10. 1016/j. conbuildmat. 2016. 06. 064.

[4] Chen J K, Jiang M Q, Zhu J. Damage evolution in cement mortar due to erosion of sulphate[J]. *Corrosion Science*, 2008, **50**(9): 2478−2483. DOI:10. 1016/j. corsci. 2008. 05. 021.

[5] Zeng G W, Yang X H, Yin A Y, et al. Simulation of damage evolution and crack propagation in three-point bending pre-cracked asphalt mixture beam[J]. *Construction and Building Materials*, 2014, **55**: 323−332. DOI:10. 1016/j. conbuildmat. 2014. 01. 058.

[6] Liu C, Xie D Q, She W, et al. Numerical modelling of elastic modulus and diffusion coefficient of concrete as a three-phase composite material[J]. *Construction and Building Materials*, 2018, **189**: 1251−1263. DOI:10. 1016/j. conbuildmat. 2018. 08. 191.

[7] Da B, Yu H F, Ma H Y, et al. Research on compression behavior of coral aggregate reinforced concrete columns under large eccentric compression loading[J]. *Ocean Engineering*, 2018, **155**: 251−260. DOI:10. 1016/j. oceaneng. 2018. 02. 037.

[8] Han S H, Park W S, Yang E I. Evaluation of concrete durability due to carbonation in harbor concrete structures[J]. *Construction and Building Materials*, 2013, **48**: 1045−1049. DOI:10. 1016/j. conbuildmat. 2013. 07. 057.

[9] Da B, Yu H F, Ma H Y, et al. Reinforcement corrosion research based on electrochemical impedance spectroscopy for coral aggregate seawater concrete in a seawater immersion environment[J]. *Journal of Testing and Evaluation*, 2020, **48**(2): 20180197. DOI:10. 1520/jte20180197.

[10] Kakooei S, Akil H M, Dolati A, et al. The corrosion investigation of rebar embedded in the fibers reinforced concrete[J]. *Construction and Building Materials*, 2012,

35: 564−570. DOI:10. 1016/j. conbuildmat. 2012. 04. 051.

[11] Da B, Yu H F, Ma H Y, et al. Factors influencing durability of coral concrete structure in the South China sea[J]. *Journal of the Chinese Ceramic Society*, 2016, **44**(2): 253−260. DOI:10. 14062/j. issn. 0454-5648. 2016. 02. 11. (in Chinese)

[12] Da B, Yu H F, Ma H Y, et al. Chloride diffusion study of coral concrete in a marine environment[J]. *Construction and Building Materials*, 2016, **123**: 47−58. DOI:10. 1016/j. conbuildmat. 2016. 06. 135.

[13] Wang J, Feng P, Hao T Y, et al. Axial compressive behavior of seawater coral aggregate concrete-filled FRP tubes[J]. *Construction and Building Materials*, 2017, **147**: 272−285. DOI:10. 1016/j. conbuildmat. 2017. 04. 169.

[14] Da B, Yu H F, Ma H Y, et al. Reinforcement corrosion research based on the linear polarization resistance method for coral aggregate seawater concrete in a marine environment[J]. *Anti-Corrosion Methods and Materials*, 2018, **65**(5): 458−470. DOI:10. 1108/acmm-03-2018-1911.

[15] Da B, Yu H F, Ma H Y, et al. Influence of inhibitors on reinforced bar corrosion of coral aggregate seawater concrete[J]. *Journal of Chinese Society for Corrosion and Protection*, 2019, **39**(2): 152−159. DOI:10. 11902/1005. 4537. 2018. 040. (in Chinese)

[16] Silva R V, de Brito J, Dhir R K. Establishing a relationship between modulus of elasticity and compressive strength of recycled aggregate concrete[J]. *Journal of Cleaner Production*, 2016, **112**: 2171−2186. DOI:10. 1016/j. jclepro. 2015. 10. 064.

[17] Tan Y S, Yu H F, Mi R J, et al. Compressive strength evaluation of coral aggregate seawater concrete (CAC) by non-destructive techniques[J]. *Engineering Structures*, 2018, **176**: 293−302. DOI:10. 1016/j. engstruct. 2018. 08. 104.

[18] Li Y, Liu X F, Li J Q. Bond properties of FRP-concrete interface with nano-modified epoxy resin under wet-dry cycles[J]. *KSCE Journal of Civil Engineering*, 2017, **21**(4): 1379−1385. DOI:10. 1007/s12205-016-0921-7.

[19] Song Z J, Jiang L H, Liu J Z, et al. Influence of cation type on diffusion behavior of chloride ions in concrete[J]. *Construction and Building Materials*, 2015, **99**: 150−158. DOI:10. 1016/j. conbuildmat. 2015. 09. 033.

[20] Wang J B, Niu D T, Song Z P. Damage layer thickness and formation mechanism of shotcrete with and without steel fiber under sulfate corrosion of dry-wet cycles by ultrasound plane testing method[J]. *Construction and Building Materials*, 2016, **123**: 346−356. DOI:10. 1016/j. conbuildmat. 2016. 06. 146.

[21] Jin Z Q, Zhao X, Zhao T J, et al. Chloride ions transportation behavior and binding capacity of concrete exposed to different marine corrosion zones[J]. *Construction and Building Materials*, 2018, **177**: 170−183. DOI:10. 1016/j. conbuildmat. 2018. 05. 120.

[22] Yang L M, Yu H F, Ma H Y, et al. Resistance of concrete to magnesium sulfate attack under combined action of carbonation and dry-wet cycles[J]. *Acta Materiae Compositae Sinica*, 2012, **29**: 127−133. DOI:10. 13801/j. cnki. fhclxb. 2012. 05. 020. (in Chinese)

[23] Gowripalan N, Mohamed H M. Chloride-ion induced corrosion of galvanized and ordinary steel reinforcement in high-performance concrete[J]. *Cement and Concrete Research*, 1998, **28**(8): 1119 − 1131. DOI:10. 1016/ S0008-8846(98)00090-8.

[24] Shaheen F, Pradhan B. Influence of sulfate ion and associated cation type on steel reinforcement corrosion in concrete powder aqueous solution in the presence of chloride ions[J]. *Cement and Concrete Research*, 2017, **91**: 73 − 86. DOI:10. 1016/j. cemconres. 2016. 10. 008.

[25] Liu J Z, Geng J D, Wang H, et al. Influence of nitrite on chemical composition of passivation film of steel bars under the coupling effects of carbonization and chloride [J]. *Anti-Corrosion Methods and Materials*, 2019, **66** (2): 230 − 235. DOI:10. 1108/acmm-09-2018-1999.

干湿-碳化耦合作用对全珊瑚海水混凝土耐久性的影响

达　波[1,2,3,4]　　余红发[5]　　麻海燕[5]　　窦雪梅[5]　　吴彰钰[5]　　陈　岩[1]

(¹ 河海大学港口海岸与近海工程学院,南京 210098)
(² 河海大学长江保护与绿色发展研究院,南京 210098)
(³ 南通河海大学海洋与近海工程研究院,南通 226300)
(⁴ 河海大学海岸灾害及防护教育部重点实验室,南京 210098)
(⁵ 南京航空航天大学土木工程系,南京 210016)

摘要:通过对不同强度等级的全珊瑚海水混凝土(CASC)进行海水干湿循环试验和海水干湿-碳化耦合循环试验,以表面状态、质量损失率、动弹性模量、超声波波速、立方体抗压强度为评价指标,研究干湿循环、碳化和干湿-碳化耦合作用对 CASC 耐久性的影响. 结果表明:干湿循环、干湿-碳化耦合作用下,CASC 的质量损失率均随着侵蚀时间的延长而逐渐增加,先期比较平缓,增长幅度不大,经过 10 次循环后,其质量损失率的增长幅度明显增大;而 CASC 的动弹性模量和超声波波速均随着循环次数的增加逐渐降低,经过 6 次循环后,其速率趋于平缓,表面有微损伤;与初始 28 d 立方体抗压强度相比,CASC 的立方体抗压强度下降幅度为 8.8% ~11.0%. 干湿循环和碳化作用对 CASC 的海水侵蚀均有加速作用,干湿循环促进盐析现象的产生,加快混凝土的破坏. 因此,干湿-碳化耦合作用加速 CASC 的破坏.

关键词:全珊瑚海水混凝土;干湿循环;干湿-碳化耦合作用;质量损失率;动弹性模量;超声波波速

中图分类号:TU528